MATEC Web of Conferences **14**, 11003 (2014)
DOI: 10.1051/matecconf/20141411003

Numerical simulation of AM1 microstructure

Luc Rougier[1,2], Alain Jacot[1,3], Charles-André Gandin[3], Paolo Di Napoli[1], Damien Ponsen[2], and Virginie Jaquet[2]

[1] LSMX, Ecole Polytechnique Fédérale de Lausanne, 1015 Lausanne, Switzerland
[2] Snecma-SAFRAN Group, Service YQGC, 92702 Colombes, France
[3] Calcom-ESI SA, Parc Scientifique, Ecole Polytechnique Fédérale de Lausanne, 1015 Lausanne, Switzerland
[4] CEMEF UMR CNRS, MINES ParisTech, 06904 Sophia-Antipolis, France

Abstract. A modelling approach is developed for the description of microstructure formation in the industrial AM1 Ni-base superalloy. Solidification and homogenization simulations are first carried out using a microsegregation model, before using the local compositions as an input for precipitation calculations, in order to characterize the influence of segregation on precipitation. First, the precipitation model was validated by comparing simulated and measured evolutions of the average precipitate radius during isothermal heat treatments at 1100 °C and 1210 °C. The chained microsegregation and precipitation simulations indicate that the global sequences of precipitation events remains are qualitatively the same at the different locations in the microstructure, but the growth and dissolution kinetics are strongly influenced by the local compositions. Local supersaturations have a larger effect on the average radius of the precipitates than certain stages of the precipitation heat treatment.

Introduction

Ni-base superalloys are widely used for aeronautical applications due to their outstanding mechanical properties at elevated temperatures. This behavior is strongly dependent on the fraction and average size of the hardening γ' precipitates in the γ matrix. In the as-cast state, the presence of residual γ/γ' eutectic in the interdendritic areas and high composition gradients in the primary γ phase are not desired since they do not allow to reach the optimal properties of the alloys. Thus, heat treatments are performed to dissolve the eutectics, homogenize the composition in the primary solid, and then, during ageing at lower temperature, form γ' precipitates with a controlled size in the supersaturated γ matrix. The goal of this work is to study the effect of an incomplete solution heat treatment on the spatial distribution of the γ' precipitates in the supersaturated γ matrix. For this, microsegregation and precipitation models are applied to the industrial AM1 superalloy.

Microsegregation can be simulated using analytical models, such as the Scheil-Gulliver model or back-diffusion models [1]. However, the dissolution of the interdendritic eutectic and the evolution of composition profiles in the primary phase during the solution heat treatment cannot be calculated with this approach. Another important feature of the Ni-based superalloys is the so-called cross-diffusion, which is the influence of the concentration gradient of a given chemical species on the flux of the other ones. For all these reasons, numerical models are preferred to simulate the solidification and heat treatment of Ni-base superalloys. Among them, phase-field modelling is potentially the most accurate. The formulation of the model enables to include the contributions of the anisotropic interfacial energy and elastic effects, which allows for the prediction of the three-dimensional morphology of the γ dendrites [2]. However, this approach is computationally very intensive and requires a difficult identification of the physical parameters. The prediction of the composition profiles and the evolution of the phase fractions can be simplified using one-dimensional models such as DICTRA [3] or the pseudo-front tracking technique (PFT) [4,5]. In the present study, the PFT approach was selected for its ability to describe the influence of back diffusion on the dissolution of eutectic phase mixtures.

Precipitation can be modeled using methods based on the evolution of the mean radius [6–8] or by calculating the change of the particle size distribution (PSD) at each time step [9–11]. The approaches based on the PSD are generally more flexible when multicomponent alloys are simulated, in particular when the thermal history includes several cooling/ageing steps [10]. These models allow for a direct treatment of cross-diffusion [12]. Furthermore, due to the high level of γ' formers in superalloys, the supersaturations in the γ matrix are high, which requires a correction of the diffusion lengths, as shown by Chen et al. [12] and Aaron et al. [13]. A model combining these solutions was presented in a recent contribution [14]. It was shown that the model could describe the precipitation in the ternary Ni-Al-Cr system, showing good agreement with the experimental data of Booth-Morrison et al. [15]. The model is now applied to the industrial AM1 superalloy. In addition, the influence of residual

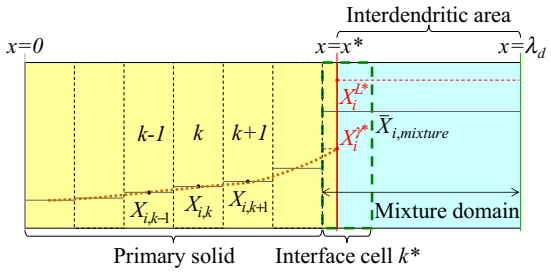

Figure 1. Schematic representation of the composition profiles calculated with the PFT model in the primary solid and interdendritic area during solidification and heat treatment.

composition heterogeneities associated with relatively short solution heat treatments is addressed through chained microsegregation and precipitation calculations.

Description of the models

Solidification/homogenization: PFT model

Primary solidification

The pseudo-front tracking (PFT) model is used to simulate the evolution of composition profiles during solidification and dissolution/homogenization heat treatments. The model is applied in one dimension, considering a domain of size λ_d, representative of half of the average dendrite arm spacing (see Fig. 1). The model is based on the numerical resolution of the diffusion equation in primary γ and a mass balance in the interdendritic region, which comprises only liquid during the first solidification stage [5,16]. The model was modified to take into account cross-diffusion, which plays an important role in Ni-base superalloys. The temporal variations of the composition are given by:

$$\frac{\partial X_i}{\partial t} = \bar{\nabla} \cdot \left(\sum_{j=1}^{nsol} D_{ij}^{\gamma} \bar{\nabla} X_j \right) \tag{1}$$

where X_j is the atomic composition of solute specie j, $nsol$ is the total number of solute elements and D_{ij}^{γ} is the diffusion coefficient of solute i with respect to composition gradient of solute j in the γ phase. The D_{ij}^{γ}'s are calculated from the values of the temperature and the average composition of the primary solid.

Equation (1) is resolved using an explicit time scheme, and a fixed grid. An interface cell is defined to track the displacement of the solid/liquid interface in the fixed mesh. Based on a local equilibrium assumption at the γ/liquid interface, the interface cell (labelled k^*) is considered to be at thermodynamic equilibrium. The composition of the liquid phase is assumed to be uniform. Neglecting the gradient in γ on the scale of the interface cell, the average composition $\bar{X}_{i,mixture}$ of the domain embedding the interface cell and the remaining liquid, hereafter named "mixture domain", is given by:

$$\bar{X}_{i,mixture} = g_{mixture}^{L} X_i^{L*} + g_{mixture}^{\gamma} X_i^{\gamma *} \tag{2}$$

where $g_{mixture}^{L}$ and $g_{mixture}^{\gamma}$ are respectively the local volume fractions of liquid and γ in the mixture domain, and X_i^{L*} and $X_i^{\gamma *}$ are the equilibrium compositions of the liquid and the γ phase, respectively.

The evolution of the average composition of the mixture domain is calculated from a mass balance and backdiffusion fluxes calculated from the concentrations gradients in primary γ at the primary γ/liquid interface. The new average composition of the mixture domain and the temperature are used as inputs for equilibrium calculations. The outputs are the new local equilibrium compositions and solid/liquid fractions in the mixture domain, which are then used to update the position of the interface, x^*. In order to improve the computational efficiency of the model, the equilibrium calculations are performed using an optimized coupling with Thermo-Calc, which was described in details by Du and Jacot [5].

Formation/dissolution of interdendritic phases and homogenization of the composition profiles in the primary solid

As cooling continues, secondary phases can start to form in the interdendritic area. Secondary phase calculations are started when the liquidus of a secondary phase, namely γ', is reached. The details of the procedure can be found in [5]. As for primary solidification, the mixture domain groups the interdendritic area and the primary phase embedded in the interface cell. Thermodynamic equilibrium and uniform compositions are also assumed to calculate the average mixture composition:

$$\bar{X}_{i,mixture} = \sum_{\nu=1}^{nph} g_{mixture}^{\nu} X_i^{\nu *} \tag{3}$$

where ν indicates the phase, nph is the total number of phases in the mixture domain, $g_{mixture}^{\nu}$ is the fraction of phase ν in the mixture and $X_i^{\nu *}$ is the equilibrium composition of phase ν in element i.

Considering that the interface between primary γ and the interdendritic area can move during eutectic formation, a supplementary condition has to be expressed to specify where the volume change of γ takes place. A parameter P_{eut} is introduced to distribute the volume increment between primary γ and the interdendritic area, i.e. as secondary γ particles:

$$P_{eut} = \Delta V_{prim}^{\gamma} / \Delta V_{tot}^{\gamma} \tag{4}$$

where ΔV_{prim}^{γ} and ΔV_{tot}^{γ} are the volume increments of primary γ, and the total volume variation of γ during the time-step, respectively.

The value of P_{eut} is a parameter of the model. It describes the growth mode of the eutectic: P_{eut} =1 corresponds to a divorced eutectic, whereas $P_{eut} = 0$ represents a coupled eutectic. The variations of compositions in primary γ are calculated in the same way as for the primary solidification. When solidification is finished, the calculation can be continued to predict the evolution of the interdendritic eutectic, and the composition profiles in primary γ.

Precipitation: PSD model

The PSD model tracks the evolution of a discretized precipitate size distribution. For each class k, which

Table 1. Nominal composition [at%] of AM1.

Al	Co	Cr	Mo	Ta	Ti	W
11.82	6.64	8.68	1.25	2.66	1.51	1.80

represents a group of precipitates, specific variables are defined, such as the radius, number density, and interface compositions in γ and γ'. A Lagrangian approach is used. It consists of tracking a group of precipitates which nucleated within the same time interval, and of calculating the evolution of the above mentioned variables due to the growth/dissolution phenomena. Each class is created during the nucleation step, based on the nucleation rate, the values of the average compositions in γ, and the temperature. This approach differs from the so-called Eulerian approach, for which the class radii are fixed and the number densities in each class are computed from the growth/dissolution rates [17]. A more detailed description has been described elsewhere [14].

Results and discussion

In this study, the PFT and PSD models were applied to the industrial AM1 superalloy, which composition is summarized in Table 1. The thermodynamic and kinetic databases used for the simulations were Ni20 and MobNi2, respectively [18,19].

PFT simulations

PFT simulations were performed for three domain sizes ($\lambda_d = 20$, 100 and 250 μm) using 1D cylindrical coordinates, in order to assess the effect of λ_d on the dissolution/homogenization kinetics. P_{eut} was fixed to 0.8. $\lambda_d = 20\,\mu$m corresponds to a minimal value of half of the secondary dendrite arm spacing $\lambda_2/2$ [20,21], while $\lambda_d = 250\,\mu$m is close to the maximal values of half of the primary spacing $\lambda_1/2$. The thermal history comprises several steps: solidification is described with a constant cooling rate of $-0.2\,^\circ$C/s, down to 600 °C. The alloy is then heated up to the solutionizing temperature of 1300 °C and held during 3h. The same thermal history was used for the three abovementioned values of λ_d. This permits to investigate the effect of the characteristic size of the microstructure on the formation/dissolution of the interdendritic γ' and the homogenization kinetics of the composition profiles in primary γ.

Figure 2 shows the variations of the volume fractions of γ, γ' and liquid during solidification. The main effect of a large dendrite arm spacing λ_d is to delay the end of solidification. Solidification terminates at 1307.2 °C, 1267.4 °C and 1247.1 °C with $\lambda_d = 20\,\mu$m, 100 μm and 250 μm, respectively. As λ_d increases, the Fourier number decreases, which has for consequence to slow down the solute transfer from the interdendritic area to the primary phases and to increase the solute accumulation in the interdendritic area, which in turn decreases the local solidus temperature. The temperature of formation of γ' is however almost independent on the value of λ_d.

Figure 3 shows the normalized composition profiles for Al, in the as-cast state and after the standard homogenization/dissolution heat treatment. Al was selected for its important role in the formation of γ'. The segregation indices χ_i are shown in Fig. 4 and are given by:

$$\chi_i = sign\left(X_{i,k^*-1} - X_{i,1}\right) \frac{\max_k\left(X_{i,k}\right) - \min\left(X_{i,k}\right)}{X_i^0} \tag{5}$$

where X_i^0 is the nominal composition and $X_{i,k}$ is the composition of element i in the cell k, and $k^* - 1$ is the last cell entirely in the primary phase, close to the interface.

In the as-cast state, a maximum of Al concentration is observed near the dendrite periphery, and its amplitude increases with λ_d. This can be explained by the decrease of the Fourier number, and indicates that the diffusion kinetics become insufficient to compensate for the solubility decrease due to cooling.

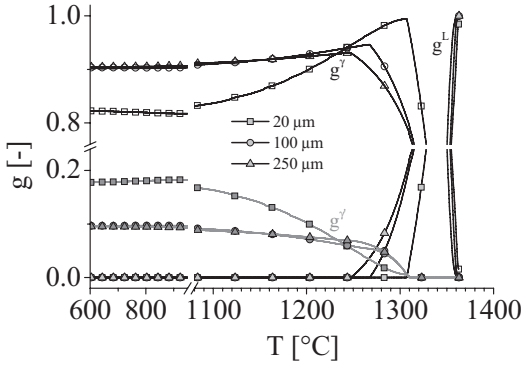

Figure 2. Variations of the volume fractions of γ, γ' and liquid with temperature during solidification.

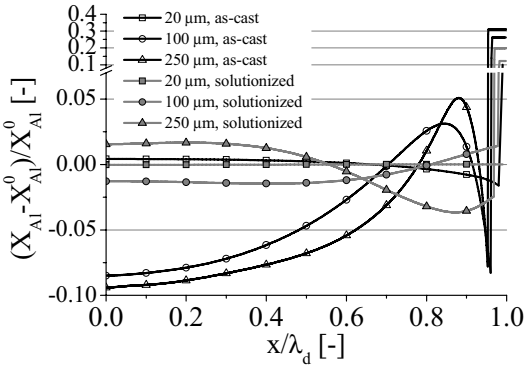

Figure 3. Normalized composition profiles of Al, as-cast and after the dissolution/homogenization heat treatment.

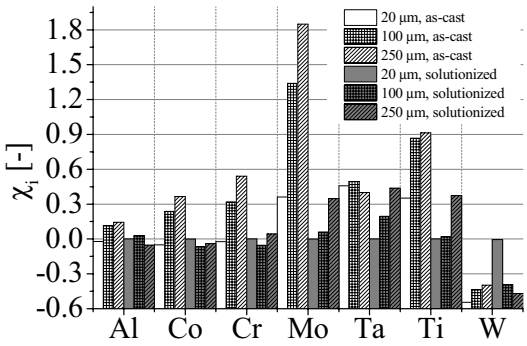

Figure 4. Segregation indices in the as-cast condition and after the dissolution/homogenization heat treatment.

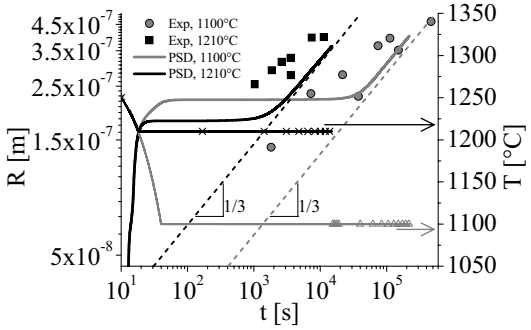

Figure 5. Average radius at 1100 °C (gray) and 1210 °C (black), obtained experimentally (symbols) and calculated with the model (continuous lines).

The dissolution/homogenization heat treatment is sufficient to completely dissolve the interdendritic γ' with $\lambda_d = 20\,\mu$m, which is not the case for $\lambda_d = 100$ and $250\,\mu$m. PFT simulations with extended dissolution/homogenization heat treatment were performed, in order to determine the required holding time for a complete dissolution for γ' with $\lambda_d = 100\,\mu$m. In this case, the interdendritic γ' is fully dissolved after roughly 5 h at 1300 °C. As shown by the evolution of the composition profiles and segregation indices, the presence of residual γ' in the interdendritic zone strongly influences the homogenization kinetics. With $\lambda_d = 20\,\mu$m, the compositions are nearly uniform after the 3 h dissolution/homogenization heat treatment. The composition profiles and segregation indices indicate a significant decrease of Al segregation after holding at 1300 °C.

Comparison of the PSD simulations with experimental results

Experimental data were collected at Snecma [22] to characterize the precipitation kinetics during isothermal ageing of AM1 at 1100 and 1210 °C. Ageing was preceded by cooling at a constant rate of -5 °C/s from a solutionizing temperature of 1300 °C. The data were obtained by Scanning Electron Microscope (SEM) observations of the precipitates after different holding times. The simulations were compared with SEM observations. For the simulations, the value of the interfacial energy, $\sigma^{\gamma/\gamma'}$, was fixed to 40 mJ · m^{-2}. The total simulated times were $2.2 \cdot 10^5$ and $1.5 \cdot 10^4$ s at T = 1100 °C and 1210 °C, respectively. The nominal composition of AM1 given in Table 1 was used for these simulations. Figure 5 shows the evolution of the volume-averaged radius $\bar{R}_V$, for both simulations and experiments. During cooling, precipitates nucleate and grow very quickly, due to the high supersaturation of the γ matrix. After a transient regime characterized by a constant average radius, the $t^{1/3}$ law, typical of steady state coarsening regime, is progressively reached. At 1100 °C, the simulations and experimental observations are in qualitative agreement. At 1210 °C, the model underestimates the average radius of the precipitates, but the qualitative evolution of $\bar{R}_V$ at long ageing times is well reproduced. The onset of precipitation has been measured by Grosdidier et al., using Differential Thermal Analysis (DTA) [23]. It varies between 1250 and 1270 °C, depending on the cooling rate. The model predicts 1236.5 °C which is in reasonable agreement, noting also that the only adjustable parameters of the nucleation model, $\sigma^{\gamma/\gamma'} = 40$ mJ · m^{-2} was determined by a trade-off between the obtained average radii and the temperature of starting precipitation.

Table 2. Local compositions [at%] used in calculations X0− and X0+.

	Al	Co	Cr	Mo	Ta	Ti	W
X0−	11.67	6.87	8.98	1.21	2.33	1.50	2.16
X0+	11.99	6.44	8.51	1.23	2.84	1.53	1.45

Chained microsegregation and precipitation simulations: Effect of the residual segregation on the precipitation kinetics

The profile obtained after the dissolution/homogenization treatment with $\lambda_d = 100\,\mu$m were then used for chained simulations. More precisely, the compositions at x = 0 μm and 97.8 μm were taken as alloy composition inputs in two PSD simulations. The corresponding calculations will hereafter be referred to as "X0-" and "X0+", and the corresponding compositions are summarized in Table 2. An additional "X0" calculation corresponding to the nominal composition of AM1 was also carried out as a reference.

The simulated precipitation heat treatment is made of two isothermal holdings: 5h at 1100 °C followed by 17.2h at 870 °C. The initial temperature is 1300 °C and the cooling is carried out at a rate of 5 °C/s. The total simulated time is 80'000s.

Figure 6 shows the variations of the number-averaged radius, $\bar{R}_N$, the volume-averaged radius $\bar{R}_V$, the total density n_{tot}, and the γ' volume fraction $g^{\gamma'}$ with time and temperature for the three selected compositions X0−, X0 and X0+. The global trends are similar for the three compositions. In all cases, nucleation and growth of a first population of precipitates occurs during cooling from 1300 to 1100 °C. It can be noted that a higher initial supersaturation (X0+) translates into a quicker nucleation, but leads to a lower number density of precipitates. This is due to a faster growth, which has for consequence to deplete the γ matrix and reduce the nucleation driving force more quickly. As the temperature becomes constant, the average radius does not significantly evolve. From 60 s–70 s (depending on the composition) to the end of the first temperature plateau (18040 s), the γ' fraction is constant and close to the equilibrium values. Furthermore, $\bar{R}_N$, $\bar{R}_V$, and n_{tot} do not reach the $t^{1/3}$ and t^{-1} dependencies, which indicates that the system still undergoes a rearrangement of the precipitate size distribution. For the case X0−, the lower supersaturation translates into a quicker transition to the coarsening regime, as shown by the evolution of $\bar{R}_V$ and the onset of dissolution near the end of the first plateau.

The second cooling is characterized by a second nucleation "burst", in which the total density increases dramatically. As the radius of the newly nucleated

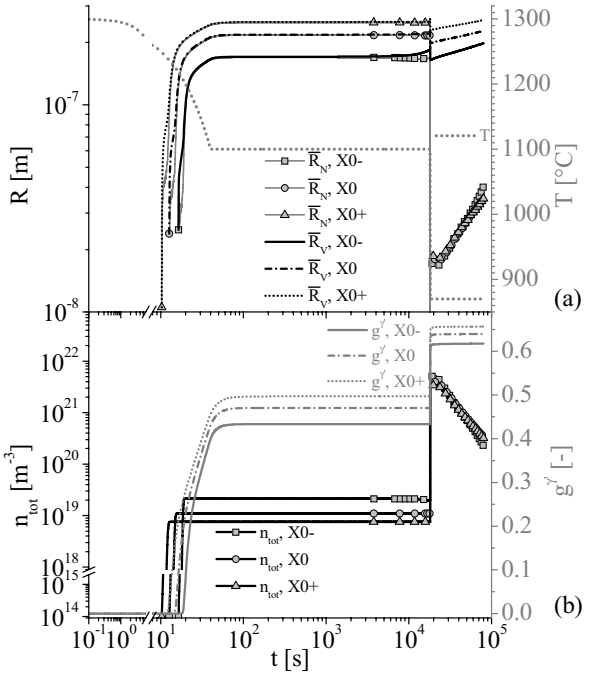

Figure 6. Calculated evolution of (a) the average precipitate radii and (b) the total precipitate density (left axis) and the precipitate fraction (right axis).

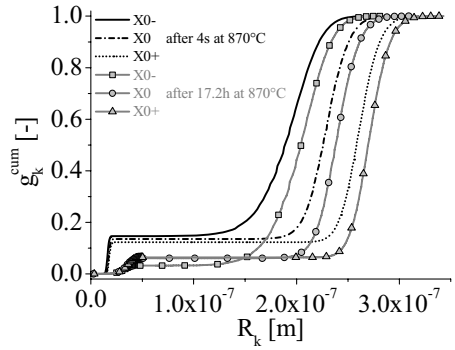

Figure 7. Normalized cumulative fraction of γ' precipitates, g_k^{cum}, versus the radii of the classes, R_k.

precipitates is small (lower than 2 nm) and despite their quick growth due to the fast resaturation of γ, they still represent a relatively minor contribution to the overall γ' volume fraction (12.3% to 14.7%, depending on the local composition). During ageing at 870 °C, these precipitates successively grow and dissolve, due to the increasing importance of coarsening as $g^{\gamma'}$ becomes close to the equilibrium value. The time exponents of $\bar{R}_N(t)$ and $n_{tot}(t)$ differ from the theoretical values of 1/3 and -1, which can be explained by the size distribution.

Figure 7 shows the normalized cumulated size distributions of the γ' precipitates after 4 s and 17.2 h at 870 °C, i.e. at the beginning and at the end of the second plateau. The cumulative volume fractions were normalized by the total volume fraction of γ'. Two populations of precipitates are observed in all cases. They are associated with the two series of nucleation events taking place during cooling from 1300 °C to 1100 °C and from 1100 °C to 870 °C. The presence of bi-modal PSDs can explain the

Table 3. Radius [m] corresponding to a relative contribution of 50% of the total γ' volume fraction at two heat treatment times and for three compositions.

Holding time at 870 °C	Composition		
	X0−	X0	X0+
4s	$1.89 \cdot 10^{-7}$	$2.26 \cdot 10^{-7}$	$2.58 \cdot 10^{-7}$
17.2h	$2.04 \cdot 10^{-7}$	$2.38 \cdot 10^{-7}$	$2.70 \cdot 10^{-7}$

deviation from the theoretical values of the coarsening time exponents. The radii corresponding to a relative volume fraction of 50% are summarized in Table 3. It can be noticed that the residual segregation has more effect than ageing at 870 °C. This is due to the fact that the biggest precipitates, nucleated during the first cooling, are the major contributors to the total fraction of γ'. They mainly grow during the first cooling/ageing sequence, which is strongly influenced by the initial supersaturation.

Conclusions

Numerical models have been developed to perform chained simulations of microsegregation, homogenization and precipitation in an industrial Ni-based superalloy. The models are coupled with Thermo-Calc and take into account the effects of high supersaturations and cross-diffusion, which are of great importance for the application to industrial alloys.

Microsegregation/homogenization simulations were carried out to calculate composition profiles in primary γ and the amount of interdendritic eutectics. The model was used to evaluate the time required for a complete dissolution of γ' in a solution heat treatment. The results show a high sensitivity of the segregation level and residual interdendritic γ' with respect to the characteristic size of the microstructure, λ_d, in both the as-cast and the homogenized states. This behavior is consistent with the variations of the Fourier numbers with λ_d. It was shown that the presence of residual γ' slows down considerably the homogenization rate in primary γ.

The precipitation model was used to describe the formation of γ' precipitates during ageing, exploiting local compositions predicted by the microsegregation model. Qualitatively, similar nucleation, growth and coarsening regimes are observed for all local compositions. However, residual segregation substantially affects the local volume fraction of precipitates and their average radius. The importance of these two quantities for mechanical properties [22,24] indicates that the mechanical behavior of the alloy is likely to be influenced by residual microsegregation for the tested conditions. The approach developed here can be applied to other Ni-base superalloys, and can be used to study modified heat treatments, and the sensitivity of different alloys with respect to the processing conditions.

Snecma-SAFRAN group is greatly acknowledged for financial support. The authors are grateful to Prof. Michel Rappaz for fruitful discussions on this project.

References

[1] J.A. Dantzig, M. Rappaz. Solidification: CRC Press, Taylor & Francis Group, 2009

[2] N. Warnken, D. Ma, A. Drevermann, R.C. Reed, S.G. Fries, I. Steinbach, Acta Mater. **57**, 5862, (2009)

[3] C. Walter, B. Hallstedt, N. Warnken, Mat. Sci. Eng. A **397**, 385, (2005)

[4] C.A. Gandin, A. Jacot, Acta Mater. **55**, 2539, (2007)

[5] Q. Du, A. Jacot, Acta Mater. **53**, 3479, (2005)

[6] J.S. Langer, A.J. Schwartz, Phys. Rev. A, **21**, 948, (1980)

[7] I.M. Lifshitz, V.V. Slyozov. J. Phys. Chem. Solids **19**, 35, (1961)

[8] C. Wagner. Z. Elektrochem. **65**, 581, (1961)

[9] R. Kampmann, R. Wagner, In: Haasen P, Gerold V, Wagner R, Ashby Michael F, editors. Decomposition of Alloys: The Early Stages. Oxford: Pergamon Press, 1984, 91

[10] M. Perez, M. Dumont, D. Acevedo-Reyes. Acta Mater. **56**, 2119, (2008)

[11] P. Maugis, M. Gouné. Acta Mater. **53**, 3359, (2005)

[12] Q. Chen, J. Jeppsson, J. Agren. Acta Mater. **56**, 1890, (2008)

[13] H. Aaron, D. Fainstein, G. Kotler. J. Appl. Phys. **41**, 4404, (1970)

[14] L. Rougier, A. Jacot, C.-A. Gandin, P. Di Napoli, P.-Y. Théry, D. Ponsen, V. Jaquet, Acta Mater. **61**, 6396, (2013)

[15] C. Booth-Morrison, J. Weninger, C.K. Sudbrack, Z. Mao, R.D. Noebe, D.N. Seidman, Acta Mater. **56**, 3422, (2008)

[16] A. Jacot, M. Rappaz, Acta Mater. **50**, 1909, (2002)

[17] O.R. Myhr, Ø. Grong, Acta Mater. **48**, 1605, (2000)

[18] Ni20: Ni Base Alloys Database version NI20, http://www.thermocalc.com

[19] MobNi2: TCS Ni-alloys Mobility Database v2.0 http://www.thermocalc.com

[20] B.C. Wilson, E.R. Cutler, G.E. Fuchs, Mat. Sci. Eng. A **479**, 356, (2008)

[21] H. Ben Hamouda, PhD Thesis, MINES ParisTech-CEMEF, Sophia-Antipolis, France, 2012

[22] C. Peyroutou, R. Tintiller, Internal report (1993)

[23] T. Grosdidier, A. Hazotte, A. Simon, Mat. Sci. Eng. A, **256**, 183, (1998)

[24] F. Diologent, P. Caron, Mat. Sci. Eng. A, **385**, 245, (2004)